

Article

# Stabilization and Speed Control of a Permanent Magnet Synchronous Motor with Dual-Rotating Rotors

Yichang Zhong <sup>1,2</sup>, Shoudao Huang <sup>1</sup>  and Derong Luo <sup>1,\*</sup>

<sup>1</sup> College of Electrical and Information Engineering, Hunan University, Changsha 410082, China; hlzyc@hnu.edu.cn (Y.Z.); hsd1962@hnu.edu.cn (S.H.)

<sup>2</sup> College of Electrical and Information Engineering, Hunan Institute of Engineering, Xiangtan 41004, China

\* Correspondence: hldr@hnu.edu.cn; Tel.: +86-731-8882-2461

Received: 9 September 2018; Accepted: 15 October 2018; Published: 17 October 2018



**Abstract:** The permanent magnet synchronous motor (PMSM) with dual-rotating rotors is a typical nonlinear multi-variable coupled system. It is sensitive to load disturbances and the change of interior parameters. The traditional proportional-integral (PI) controller is widely used in the speed control of a motor because of its simplicity; however, it cannot meet the requirements needed for high performance. In addition, when the loads of both of the rotors change, it is difficult to ensure that the system runs stably. With an aim to mitigate these problems, a method called master-slave motor control is proposed to guarantee the stability of the motor system in all cases. And then, a speed controller is designed to eliminate the influence of uncertain terms. The proposed control strategy is implemented both in simulations and in experiments. Through the analysis and comparison of the proportional-integral (PI) controller and the sliding-mode controller, the effectiveness of the proposed control strategy is validated.

**Keywords:** permanent magnet synchronous motor (PMSM) with dual-rotating rotors; stability analysis; master-slave motor control; speed controller; sliding-mode control (SMC)

## 1. Introduction

The permanent magnet synchronous motor (PMSM) has been widely utilized in different industry fields because of its superior power density, high torque, and high efficiency [1,2]. Similar to the traditional PMSM, the PMSM with dual-rotating rotors also has characteristics such as high efficiency, high torque capability, and compact size, and has been a topic of research in the last couple of decades [3,4]. Thus, the PMSM with dual-rotating rotors has been widely used in various applications such as electric ships, UVs (underwater vehicles), hybrid electric vehicles, and airplane propulsion due to its compact construction and high-power density [5,6].

Usually, a motor with multiple rotating rotors can be looked at as multiple traditional motors connected in parallel or in series [4,7–9]. For the topology of the motor with dual-rotating rotors, the two working surfaces of the stator core are used and the winding end portion is greatly shortened, which allows the machine to exploit a much higher percentage of the stator winding for the production of the machine torque, compared with conventional machines. Although the PMSM with dual-rotating rotors has these advantages, it also faces an unavoidable problem of how to keep the speed of both rotors synchronized when the load changes. For the traditional PMSM, the solution for synchronism is that the electromagnetic torque must be equal to the load torque, and the rotor rotation speed must be synchronized with the magnetic field rotation speed. Similarly, for the PMSM with dual-rotating rotors, each rotor's rotation speed should also be synchronized with the magnetic field rotation speed. For the

multiple induction motors system, scholars have adopted different control methods to guarantee the stability in existing studies [7–12]. Scholars have also studied the stability and speed synchronization of the multiple PMSMs system. In order to guarantee the stable operation of the multiple motors, connected in parallel, Bidart et al. [13] proposed a scheme of selecting one of the motors as the master motor. Based on an improved cross-coupling structure [14], Wei C. et al. adopted a fuzzy self-adjusting cross-coupling control structure to control speed synchronism for the multiple permanent magnet synchronous motors that were connected in parallel. For the multi-PMSM system connected in series, Chiasson et al. [15] presented a strategy to control each motor's quadrature current. For the PMSM with dual-rotating rotors, the load of each rotor may change. Accordingly, the stable operation of the motor system is the major premise for speed synchronization. Chen and Luo [16] analyzed the unstableness of the system when unbalanced loads were applied to the motor. Zhong et al. [17] discussed three operating situations, in case of load variation, of the PMSM with both rotors. Therefore, the first goal of this work is to solve the problem of how to make the PMSM with dual-rotating rotors operate stably when both loads are unbalanced.

With its simple structure, good stability, high reliability, and easy parameter adjustment, the proportional-integral (PI) control technology is very popular, and is very effective for the current control of PMSM when a precise model can be obtained [18]. However, the uncertainties of PMSM, caused by external load torque disturbances and internal parametric variations, negatively influence the obtainment of a precise model. To improve system robustness and obtain high performance, it is necessary to design advanced controllers. In the past decades, many scholars have designed novel controllers, to improve control performance, by using some nonlinear techniques, such as robust control [19,20], sliding-mode control (SMC) [21–23], intelligent control [24,25], self-learning technology [26,27], and so on. In addition, some advanced control algorithms have also been studied in the motor drive system. Sun et al. [28] proposed a neural network inverse scheme to achieve fast-response and high-precision performance in the case of external disturbance and parameter uncertainty. In [29], internal model control was proposed to improve the robustness of the motor system. In [30], Sun et al. realized the speed observer through a speed-sensorless control scheme and effectively rejected the influence of speed detection. Among these nonlinear control techniques, SMC technology is a popular nonlinear control to handle disturbances, and it exhibits advantages such as quick response, good robustness, and simple implementation. However, the conventional SMC usually uses large control gains to control the motor system, which may generate some undesired chattering when the motor system is in the sliding mode. The proposed sliding-mode controller adopts the boundary layer technique, which can avoid the use of large control gains for the control system and, thus, eliminate the system chattering to obtain high control performance [2,18]. Therefore, to deal with the non-periodic disturbance of the system and improve the tracking performance, a speed controller via SMC is developed. To eliminate the chattering, a boundary layer technique [2,18] is usually adopted and, subsequently, the application of the proposed SMC on the speed controller is shown.

The paper is organized as follows: In Section 2, the three-dimensional (3D) model of the motor is described, and the operation principle of the motor is introduced; Section 3 describes the master-slave motor control method, which guarantees the stability of the motor drive system in all cases, and the speed controller via SMC is designed; in Section 4, in order to demonstrate the effectiveness of the proposed control scheme, the simulations and experimental results are derived and discussed; and, finally, the paper is concluded in Section 5.

## 2. Three-Dimensional (3D) Model and Operation Principle

As is illustrated in Figure 1a, the three-dimensional (3D) model of the PMSM with dual-rotating rotors is shown. Figure 1a shows that the two working surfaces of the stator iron were both used and the winding end portion was greatly shortened, which allowed the motor to achieve higher efficiency and compactness in comparison to conventional motors. As shown in Figure 1a, the PMSM with

dual-rotating rotors was constructed from three main parts: Rotor 1 with permanent magnet (PM), Rotor 2 with permanent magnet (PM), and a stator which is fed by the voltage source inverter (VSI). The PMSM with dual-rotating rotors can be considered as having both permanent magnet motors connected in series. For convenience of explanation, the PMSM with dual-rotating rotors can be regarded as being two PM motors connected in series; motor 1 and motor 2 are named. In Figure 1a, motor 1 consists of half of the stator (stator iron and toroidal windings) and rotor 1. Similarly, motor 2 consists of the other half of the stator and rotor 2.

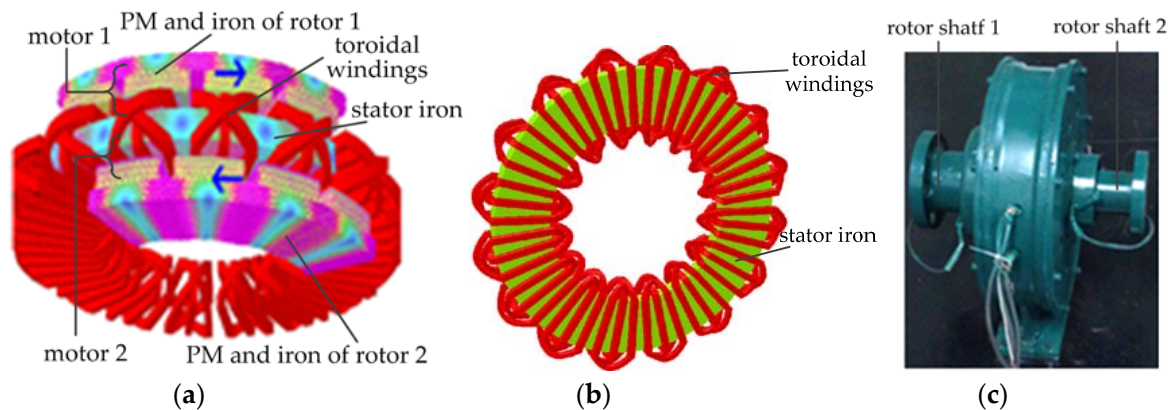


**Figure 1.** Model of the motor. (a) 3D model; (b) overview of the stator; and (c) the prototype of the motor.

As is illustrated in Figure 1b, the overview of the stator is shown. In order for both of the rotors to rotate in the anti-direction, the phase order of toroidal windings must be opposite. The opposite phase order can be developed through shifting two phase windings (phase B and C). When the three-phase power is supplied to the motor, both magnetic fields can develop and rotate in opposite directions at the two sides of the stator. The rotor flux separately interacts, with respective rotating fields, to develop the electromagnetic torques which drive the two rotors to run in the opposite direction [4,16,17]. The prototype of the motor is shown in Figure 1c.

### 3. Mathematical Modeling and Control Methodology

In order to facilitate the description of the proposed control strategy in the paper, it is necessary to introduce the mathematical model of the motor, the speed controller designed based on SMC, and the study of stable operation.

#### 3.1. Mathematical Modeling

For mathematical modeling, it was necessary to introduce the d-q1 synchronization reference frame (for motor 1) and d-q2 (for motor 2) synchronization reference frame. The two rotors rotated in the opposite direction, and the armature magnetic fields also rotated in the opposite direction. For both rotors, the directions of the two angular speeds are the same [4,16,17], namely that the rotation directions for the two d-q reference frames in space are the same. Therefore, both rotors can be put in a uniform d-q coordinate frame for analysis.

In order to explain the mathematical modeling, it was assumed that the magnetic flux of the two PM motors was not saturated, the magnetic field was sinusoidal, and the influence of the magnetic hysteresis was negligible. Because of being connected in series, the stator voltage equations of the PMSM with dual-rotating rotors can be expressed as follows:

$$\begin{aligned}
 u_d &= u_{d1} + u_{d2} \\
 &= (R_{s1}i_{d1} + L_d \frac{di_{d1}}{dt} - L_d i_{q1} \omega_1) + (R_{s2}i_{d2} + L_d \frac{di_{d2}}{dt} - L_d i_{q2} \omega_1) \\
 &= 2R_s i_d + 2L \frac{di_d}{dt} - Li_q (\omega_1 + \omega_2)
 \end{aligned} \tag{1}$$

$$\begin{aligned}
 u_q &= u_{q1} + u_{q2} \\
 &= (R_{s1}i_{q1} + L_q \frac{di_{q1}}{dt} + L_q i_{d1} \omega_1 + \psi \omega_1) + (R_{s2}i_{q2} + L_q \frac{di_{q2}}{dt} + L_q i_{d2} \omega_2 + \psi \omega_2) \\
 &= 2R_s i_q + 2L \frac{di_q}{dt} + Li_d (\omega_1 + \omega_2) + \psi (\omega_1 + \omega_2)
 \end{aligned} \tag{2}$$

where  $\psi$  is the permanent magnet flux linkage,  $\omega_1$  is the electrical angular speed of rotor 1,  $\omega_2$  is the electrical angular speeds of rotor 2. There is  $R_{s1} = R_{s2} = R_s$  and  $L_d = L_q = L$ , where  $R_s$  is the stator resistance and  $L_d$  and  $L_q$  are the d-q axes stator inductances, respectively. In (1) and (2), the subscript  $n = 1$  or  $n = 2$  indicates whether the quantity corresponds to the d-q1 reference frame (for motor 1) or d-q2 reference frame (for motor 2).

The mechanical model of the two motors can be described as follows:

$$\begin{cases} J\dot{\omega}_1 = T_{e1} - T_{l1} \\ \dot{\theta}_1 = \omega_1 \end{cases} \tag{3}$$

$$\begin{cases} J\dot{\omega}_2 = T_{e2} - T_{l2} \\ \dot{\theta}_2 = \omega_2 \end{cases} \tag{4}$$

where  $J$  is the moment of inertia.  $T_{l1}$  and  $T_{l2}$  and  $T_{e1}$  and  $T_{e2}$  are the load torques and the electromagnetic torques, respectively.  $\theta_1$  and  $\theta_2$  are the angular positions of both rotors.

Using the method of field-oriented control (FOC), the d-axis current should be controlled to be zero, namely  $i_d = 0$ . When balanced load torques ( $T_{l1} = T_{l2}$ ) were applied to both rotors, both of the rotors rotated at the same speed during the steady operation. For the motor system, there was  $\omega_1 = \omega_2 = \omega$  and  $\theta_1 = \theta_2 = \theta$ . Meanwhile, the load torque angles  $\delta_1$  and  $\delta_2$  satisfied the relationship of  $\delta_1 = \delta_2 = 90^\circ$ . The electromagnetic torque mathematic model can be expressed as

$$T_{e1} = T_{e2} = \frac{3}{2} p \psi i_q \tag{5}$$

where  $p$  is the number of pole pairs. Figure 2a demonstrates the vector diagram in the case of balanced load torques ( $T_{l1} = T_{l2}$ ).

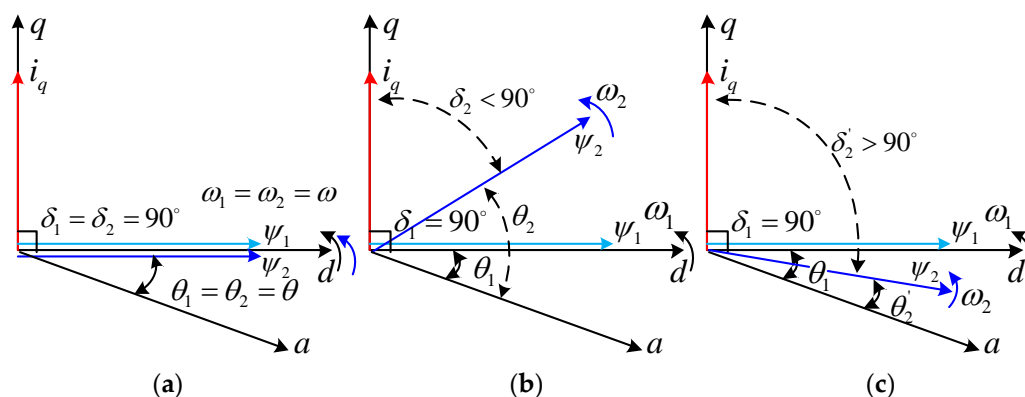


**Figure 2.** Vector diagram for the motor. (a) Case 1:  $T_{l1} = T_{l2}$ ; (b) case 2:  $T_{l1} > T_{l2}$ ; and (c) case 3:  $T_{l1} < T_{l2}$ .

When the load torque is suddenly applied to the rotor, the rotation speed of the rotor may change, which makes  $\omega_1$  and  $\omega_2$  unequal. Consequently, the next goal was to drive both rotors to rotate at the same speed in a steady state. Using the method of field-oriented control (FOC), the flux linkage of

rotor 1 ( $\psi_1$ ) was oriented. Therefore, motor 1 (called the ‘master motor’) could be controlled so that the torque angle of rotor 1 satisfied the relationship of  $\delta_1 = 90^\circ$ . As shown in Figure 2b, the  $\psi_2$  led the  $\psi_1$  when  $T_{l1} > T_{l2}$  and there was  $\delta_2 < 90^\circ$ . But when  $T_{l1} < T_{l2}$ , the  $\psi_2$  lagged behind the  $\psi_1$ , and there was  $\delta_2 > 90^\circ$ , as shown in Figure 2c. Consequently, the electromagnetic torque should be rewritten as follows:

$$T_{e1} = \frac{3p\psi}{2}i_q (\delta_1 = 90^\circ, \text{ for motor 1}) \quad (6)$$

$$T_{e2} = \frac{3p\psi}{2}i_q \sin \delta_2 (\text{when } T_{l1} > T_{l2}, \text{ for motor 2}) \quad (7)$$

$$T'_{e2} = \frac{3p\psi}{2}i_q \sin \delta'_2 (\text{when } T_{l1} < T_{l2}, \text{ for motor 2}) \quad (8)$$

### 3.2. Stability Analysis of the PMSM System

The proposed motor is distinguished by both of its rotors rotating at the same rate as the magnetic field which drives it. This synchronism has to always be respected whenever the load torques change. When the load torque ( $T_{li}$ ) is applied to the rotor, to ensure the stability of the PMSM with dual-rotating rotors, the electromagnetic torque must tend towards this value:  $T_{ei} = T_{li}$ . The subscript  $i = 1$  or  $i = 2$  suggests whether the quantity corresponds with motor 1 or motor 2.

As described above, motor 1 was the master motor while motor 2 was the slave motor. For the master motor (motor 1),  $\psi_1$  was always oriented, and there was  $T_{e1} = \frac{3p\psi}{2}i_q$  and  $\delta_1 = 90^\circ$ . For the slave motor (motor 2), the following is mainly to discuss whether its electromagnetic torque was equal to its load torque.

Case 1:  $T_{l1} = T_{l2}$ . For motor 1,  $\psi_1$  was oriented, and there was  $T_{e1} = \frac{3p\psi}{2}i_q$  and  $\delta_1 = 90^\circ$ . In the stable state, both motors had the same mechanical rotor speed:  $\omega_1 = \omega_2 = \omega$ . As shown in Figure 2a, the load torque angles  $\delta_1$  and  $\delta_2$  satisfied the relationship of  $\delta_1 = \delta_2 = 90^\circ$ .

The master motor was motor 1, running in stable state:  $\Rightarrow T_{e1} = \frac{3p\psi}{2}i_q = T_{l1}$ .

The slave motor was motor 2. According to Equation (5),  $T_{e2} = \frac{3p\psi}{2}i_q = T_{e1} = T_{l1}$  can be yielded.  $\therefore T_{l1} = T_{l2}, \Rightarrow T_{e2} = T_{l2}$ .

$\therefore \Rightarrow$  Slave motor 2 was stable.

Case 2:  $T_{l1} > T_{l2}$ . Motor 1 was still the master motor, running in stable state:  $\Rightarrow T_{e1} = \frac{3p\psi}{2}i_q = T_{l1}$ .

The slave motor was motor 2. As shown in Figure 2b, rotor 2 led rotor 1, and there was  $\theta_2 > \theta_1$  and  $\delta_2 < \delta_1$  ( $\delta_1 = 90^\circ$ ). According to Equations (6) and (7), there was  $T_{e1} = \frac{3p\psi}{2}i_q$  and  $T_{e2} = \frac{3p\psi}{2}i_q \sin \delta_2$ ,  $\therefore \Rightarrow T_{e1} > T_{e2}$ . Because of  $T_{l1} > T_{l2}$ , a suitable  $\delta_2$  can always be obtained to satisfy the relationship of  $T_{e2} = T_{l2}$  in an equilibrium state.

$\therefore \Rightarrow$  The slave motor 2 was stable.

Case 3:  $T_{l1} < T_{l2}$ . As the aforementioned cases, the master motor was still motor 1, running in stable state:  $\Rightarrow T_{e1} = \frac{3p\psi}{2}i_q = T_{l1}$ .

The slave motor was motor 2. As shown in Figure 2c, rotor 2 will lag behind rotor 1, and there was  $\theta'_2 < \theta_1$  and  $\delta'_2 > \delta_1$  ( $\delta_1 = 90^\circ$ ). According to Equations (6) and (8), there was  $T_{e1} = \frac{3p\psi}{2}i_q$  and  $T'_{e2} = \frac{3p\psi}{2}i_q \sin \delta'_2$ ,  $\therefore \Rightarrow T'_{e2} < T_{e1}$ .  $\therefore T_{l1} < T_{l2}, \therefore \Rightarrow T'_{e2} < T_{l2}$ . For motor 2, its load torque was always more than its electromagnetic torque.

$\therefore \Rightarrow$  The stability of slave motor 2 cannot be guaranteed.

### 3.3. The Proposed Control Methodology

#### 3.3.1. Using the Rotor Position to Select the Master Motor

The positions of both the rotors can change when the load torques change, as mentioned above:

If there is  $T_{l1} \geq T_{l2}$ , the angular position meets  $\theta_1 \leq \theta_2$ , and motor 1 can be selected as the master motor, and motor 2 can also run stably.

If there is  $T_{l1} < T_{l2}$ , the angular position meets  $\theta_1 > \theta_2$ . If the  $\psi_1$  is oriented and the master motor is motor 1, motor 2 cannot run stably.

Therefore, the main motor can be selected by comparing the sizes of both the rotor positions. When the angular position meets  $\theta_1 > \theta_2$ , motor 2 becomes the master motor and motor 1 is the slave motor. Because of re-orienting to  $\psi_2$ , the master motor is motor 2. As a result, this situation is the same as case 2 ( $T_{l1} > T_{l2}$ ) mentioned above, in which the slave motor can run stably. In short, the motor to which the higher load torque is applied has to be chosen as the master and, accordingly, the stability of both the motors can be ensured.

### 3.3.2. Sliding-Mode Speed Controller Design

Compared with other nonlinear control methods, SMC is more insensitive to internal parameter variations and external disturbances once the system trajectory reaches, and stays on, the sliding surface. In general, the SMC design can be divided into two steps: The first step is to choose a suitable sliding-mode surface; and the second step is to design the control input so that the system trajectory is forced to the sliding-mode surface, which ensures the system satisfies the sliding-mode reaching condition that is expressed as follows:

$$s\dot{s} < 0 \quad (9)$$

where  $s$  is the sliding-mode surface.

The state variable of the system can be expressed as follows:

$$\begin{cases} x_1 = \omega^* - \omega \\ x_2 = \dot{x}_1 = -\dot{\omega} \end{cases} \quad (10)$$

where  $\omega^*$  is the desired speed, and  $\omega$  is the actual speed. Thus, the differential equations are given as follows:

$$\begin{cases} \dot{x}_1 = -\dot{\omega} \\ \dot{x}_2 = \ddot{x}_1 = -\ddot{\omega} \end{cases} \quad (11)$$

As mentioned above, motor 1 or motor 2 can be chosen as the master motor. When the master motor is motor 1, substituting Equations (3) and (5) into Equation (11), the differential Equation (11) can be rewritten as follows:

$$\begin{cases} \dot{x}_1 = -\dot{\omega}_1 = -\frac{3p\psi}{2J}i_q + \frac{1}{J}T_{l1} \\ \dot{x}_2 = \ddot{x}_1 = -\ddot{\omega}_1 = -\frac{3p\psi}{2J}\dot{i}_q \end{cases} \quad (12)$$

Similarly, if the master motor is motor 2, there is  $\omega = \omega_2$ . Substituting Equations (4) and (5) into Equation (11), then

$$\begin{cases} \dot{x}_1 = -\dot{\omega}_2 = -\frac{3p\psi}{2J}i_q + \frac{1}{J}T_{l2} \\ \dot{x}_2 = \ddot{x}_1 = -\ddot{\omega}_2 = -\frac{3p\psi}{2J}\dot{i}_q \end{cases} \quad (13)$$

For simplification, we can rewrite Equations (12) and (13). Defining  $A = \frac{3p\psi}{2J}$ , the state space expression of the motor system can be written as follows:

$$\begin{pmatrix} \dot{x}_1 \\ \dot{x}_2 \end{pmatrix} = \begin{pmatrix} 0 & 1 \\ 0 & 0 \end{pmatrix} \begin{pmatrix} x_1 \\ x_2 \end{pmatrix} + \begin{pmatrix} 0 \\ -A \end{pmatrix} \dot{i}_q \quad (14)$$

A typical sliding-mode surface can be chosen as follows:

$$s = cx_1 + x_2 \quad (15)$$

A typical sliding-mode surface can guarantee the asymptotic stability of the sliding mode, and the asymptotic rate of convergence is in direct relation with the value of  $c$ . Therefore, the control input of the system should be designed in such a way that the sliding-mode reaching condition (inequality (9)) is met. In order to improve the dynamic quality of the system, an exponential reaching law is used to design the controller. Thus, the reaching law is usually chosen as follows:

$$\dot{s} = -\eta \operatorname{sgn}(s) - ks \quad (\eta > 0, k > 0) \quad (16)$$

Taking the time derivative of the sliding-mode surface (15) yields

$$\dot{s} = c\dot{x}_1 + \dot{x}_2 = cx_2 + \dot{x}_2 \quad (17)$$

Substituting Equation (14) into Equation (17), the following equation can be obtained as follows:

$$\dot{s} = cx_2 - Ai_q \quad (18)$$

Substituting Equation (16) into Equation (18), then the following can be obtained as follows:

$$-\eta \operatorname{sgn}(s) - ks = cx_2 - Ai_q \quad (19)$$

Therefore, the control input  $i_q^*$  is designed as follows:

$$i_q^* = A^{-1} \int (cx_2 + \eta \operatorname{sgn}(s) + ks) dt \quad (20)$$

In practical application, there are undesired chattering phenomena in sliding-mode control. To improve the robustness of the motor system, the boundary layer technique [2,18] is used to eliminate the chattering caused by the  $\operatorname{sgn}$  function in (20). Therefore, the  $\operatorname{sat}$  function takes place of the  $\operatorname{sgn}$  function. The  $\operatorname{sat}$  function is as follows:

$$\operatorname{sat}(s, \delta) = \begin{cases} 1, & s > \delta \\ s/\delta, & |s| < \delta \\ -1, & s < -\delta \end{cases} \quad (21)$$

where  $\delta$  is the boundary layer and chosen to be 2. So, the control input  $i_q^*$  can be rewritten as follows:

$$i_q^* = A^{-1} \int (cx_2 + \eta \operatorname{sat}(s, \delta) + ks) dt \quad (22)$$

If the Lyapunov function  $V = \frac{1}{2}s^2$  is chosen, the following sliding condition can be derived:

$$\dot{V} = s\dot{s} = -\eta s \operatorname{sgn}(s) - ks^2 = -\eta |s| - ks^2 < 0 \quad (23)$$

According to the Lyapunov stability criterion, the designed control system is stable.

For improving the response speed and decreasing the steady state error, the absolute value of the speed error is taken into account when choosing the variable parameter in the simulation. As shown in Figure 3,  $|x_1|$  is the absolute value of the speed error, and  $n_i$  is the given comparison value,  $n_1 < n_2 < \dots < n_i$ ; and  $k_i$  is the corresponding coefficient changing with  $n_i$ ,  $k_0 < k_1 < \dots < k_i$ .

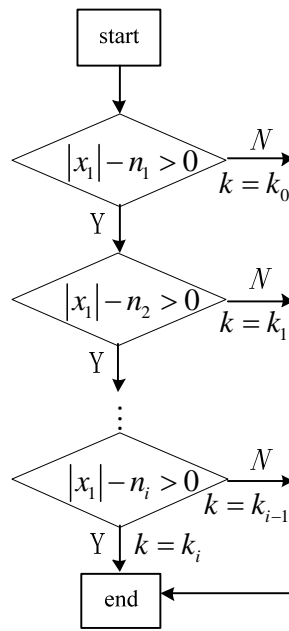


Figure 3. Flow chart of variable  $k$ .

#### 4. Simulation and Experimental Results

In this section, the simulation and experimental results are presented to demonstrate the effectiveness of the proposed control scheme. In order to compare the control performance, the traditional PI control and the proposed control method were simulated and tested. The overall block diagram for the proposed control scheme is shown in Figure 4. The overall system consisted of the proposed SMC speed controller, a Space vector pulse width modulation (SVPWM) inverter, the prototype of the motor, a position selector, and a speed selector. The angular positions of both the rotors were compared so as to generate the selection signal. According to the selection signal ( $k = 0$  means motor 1 was the master motor, and  $k = 1$  means motor 2 was the master motor), the Digital Signal Processor (DSP TMS320F28335) controller could make the right decision in the selection of the master motor. The nominal parameters of the PMSM are listed in Table 1.

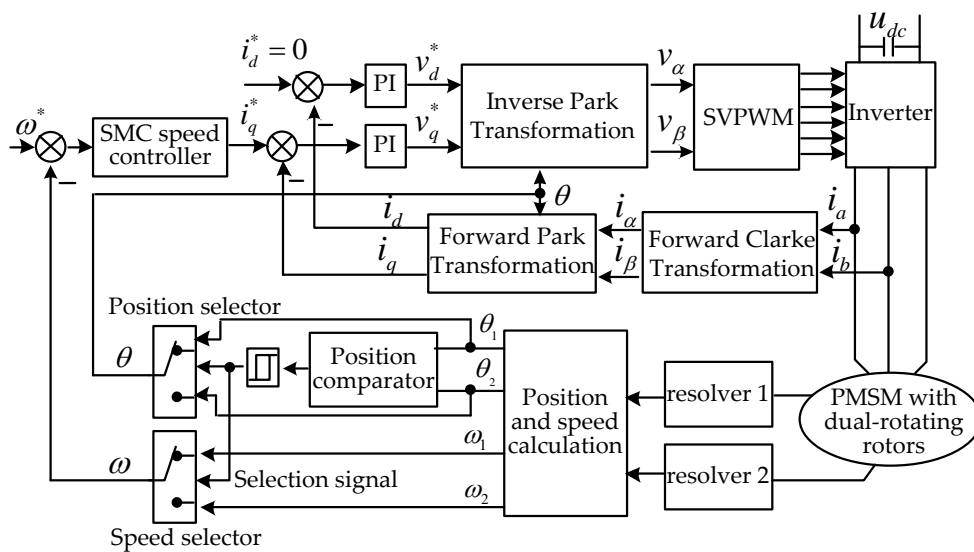
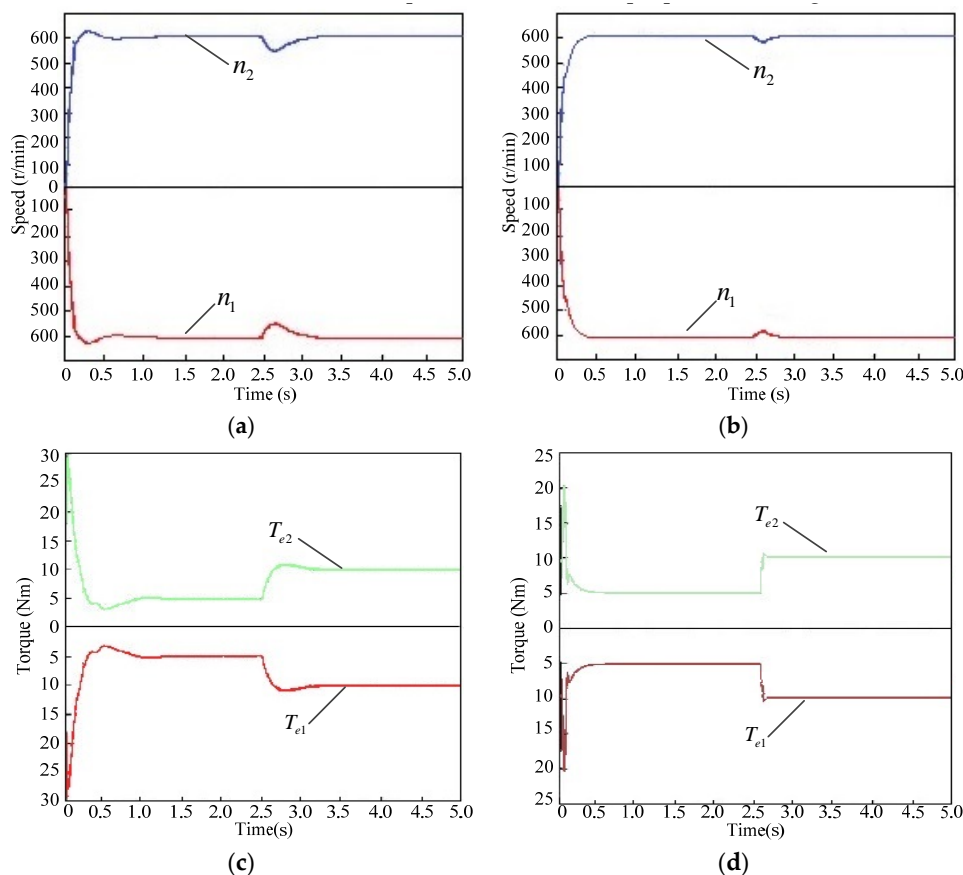


Figure 4. Overall block diagram for the proposed speed control scheme.

**Table 1.** Nominal parameters of the permanent magnet synchronous motor (PMSM) with dual-rotating rotors.

Parameters	Values	Parameters	Values
Rated power	2200 W	Nominal torque	$2 \times 10$ Nm
Specified speed	$2 \times 600$ r/min	Number of pole pairs	16
Nominal frequency	80 Hz	Stator resistance	$2 \times 1.05$ $\Omega$
DC bus voltage	300 V	d-q axis inductance	$2 \times 1.253$ mH
Phase current	5 A	Magnet thickness	8.5 mm
Stator inner diameter	300 mm	Stator outer diameter	480 mm
Rotor inner diameter	300 mm	Rotor outer diameter	480 mm

Figure 5 shows comparisons of the simulation results between the PI speed controller and the proposed SMC speed controller to demonstrate the performance improvement. From the simulation results of the two different control methods, it can be seen that the fluctuations of speed and the electromagnetic torque controlled by SMC were much smaller than those with the conventional PI speed controller. When loading the torque of both the rotors, from 5 Nm to 10 Nm at 2.5 s, it can be seen from Figure 5 that when sliding-mode control was adopted the overshoot of the speed, or the electromagnetic torque, was smaller than that of the conventional PI control. This indicated that the sliding-mode control had better robust performance, and that the dynamic performance and robustness were both improved based on the proposed SMC algorithm.

**Figure 5.** Performance comparisons under the proportional-integral (PI) speed control scheme and the sliding-mode control (SMC) speed control scheme. (a) Speed response (PI speed control); (b) speed response (SMC speed control); (c) torque response (PI speed control); and (d) torque response (SMC speed control).

The effectiveness of the proposed control scheme was investigated via experiment in the motor platform. Figure 6 shows the entire experimental platform. The experimental platform was composed of a PMSM with dual-rotating rotors controlled by a Digital Signal Processing (DSP TMS320F28335) controller, which was programmed in CCS (Code Composer System). The control algorithms, including the proposed SMC and PI controls, and the mathematical transformations, as mentioned in Figure 4, were implemented in the DSP TMS320F28335. The input terminals of the motor were connected to a three-phase power source. The load transducer was mounted on the motor rotor and the load generator was connected to the load transducer. In the experiment, the speed controller was the adopted SMC and the current controller was the adopted PI. The parameters of the two current PI controllers were the same:  $k_{pc} = 10$  and  $k_{ic} = 3.5$ . It should be noted that the PI parameters of the controller were test values after on-site commission [31]. The parameters of the SMC speed controller were  $k_0 = 25$  and  $x_1 = \omega^* - \omega$ .

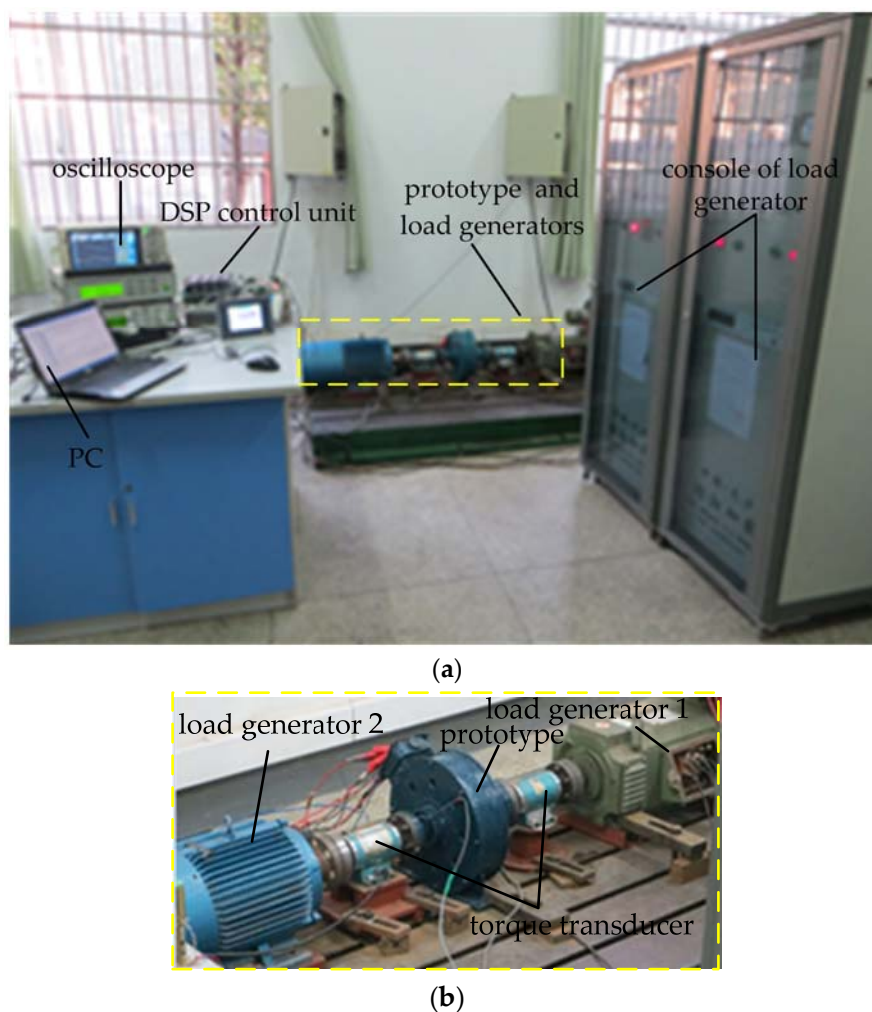


**Figure 6.** Photograph of the experimental platform. (a) Overview of the experimental set-up; and (b) overview of the prototype and the load generators.

#### 4.1. Rotor Position Alignment

In order to obtain the maximum torque angle of  $90^\circ$ , the d-axis current should be controlled to be zero when the method of field-oriented control is adopted. However, for the permanent magnet synchronous motor with dual-rotating rotors, the positions of both the rotors may not be in the same position at the beginning of the motor start-up. If a vector current is arbitrarily oriented to one rotor, the other rotor may not start simultaneously, especially when both rotors are loaded. Obviously, the

load angle of the rotor that cannot be started may just be small, which is not enough to generate adequate electromagnetic torque to drive rotor rotation.

A solution to effectively start the proposed motor was to align the position of both rotors. Firstly, a constant current vector, with certain amplitude, was applied to the stator windings and the direction of the current vector was aligned with the axis of the phase A winding. An electromagnetic field was generated by the current vector, so that both the permanent magnet rotors were attracted and rotated to the specific location of the axis of the A phase winding. It is worth mentioning that the two winding axes were not mechanically identical because of cross-displacement of windings between phase A and B. Secondly, the values of both the rotors' angular positions were read. One of the resolver's stators was removed from the motor, and then the removed resolver's stator was manually rotated an appropriate angle, where the value of the rotor's angular position was roughly equal to the value recorded by the other resolver. Lastly, the removed resolver's stator was mounted to the motor again. What is worth mentioning is that the rotor position did not need to be adjusted to any further extent.

When the proposed motor needed to be started, a current vector, as mentioned above, was supplied into the motor to align both the rotors. The time of the whole alignment process was about one or two seconds. The method of rotor position alignment for the proposed motor is practical because the load torque of the two rotors is relatively small during start-up [16,17]. Figure 7 shows the whole alignment process as mentioned above. In the initial stage of the motor start-up, it was obvious that the position of both the rotors,  $\theta_1$  and  $\theta_2$ , were not aligned. After about 1.5 seconds, both the rotors rotated in an approximately equal position and had the same angular position ( $\theta$ ), which indicated that the method of the rotor position alignment described above is feasible.

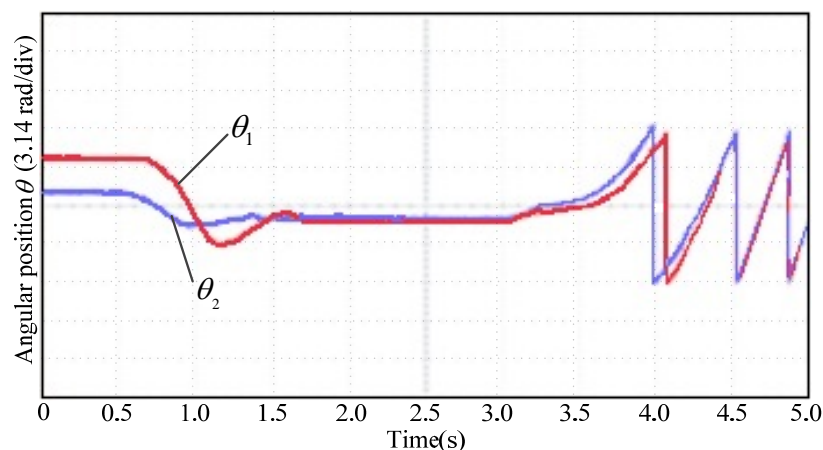
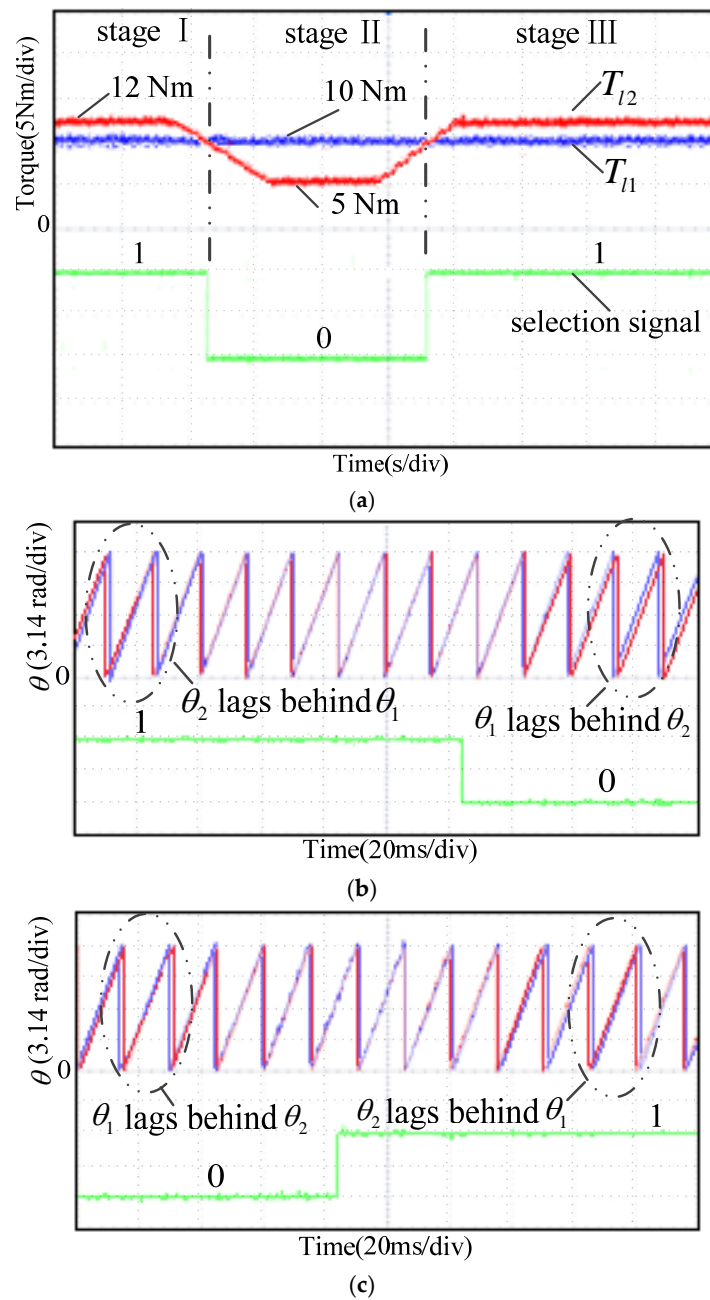


Figure 7. Rotor position alignment during the motor start-up.

#### 4.2. Master Motor Selection Experiment

The master motor selection method of comparing the rotor position was also verified by way of experiment. As mentioned above, the angular position of the motor with a higher load torque will be smaller than the angular position of the motor with a lighter load torque. The motor to which the higher load torque is applied has to be chosen as the master so that the stability of both the motors can be guaranteed. In the experiment, the load torque  $T_{11}$  remained unchanged ( $T_{11} = 10$  Nm), while the load torque  $T_{12}$  changed from 12 Nm to 5 Nm, and back to 12 Nm.

As shown in Figure 8, the experiment illustrated how the selection signal operates when the load torque changes. The whole experiment process can be divided into three stages: At stage I ( $T_{12} > T_{11}$ ), the angular position  $\theta_2$  lagged behind  $\theta_1$ , which met  $\theta_1 > \theta_2$ , and the selection signal met  $k = 1$  and the master motor was motor 2; at stage II ( $T_{11} > T_{12}$ ), the angular position  $\theta_1$  lagged behind  $\theta_2$ , which met  $\theta_2 > \theta_1$ , and the select signal changed to  $k = 0$  and thus the master motor was motor 1; at stage III ( $T_{12} > T_{11}$ ) motor 2 became the master motor again. Accordingly, it was shown that the selection signal can correctly select the master motor.



**Figure 8.** Variation of the load torque and transition of the selection signal. (a) Variation of the selection signal and load torques under different conditions; (b) variation of the selection signal (from 1 to 0) and variation of the angular position (from  $\theta_2$  lagging behind  $\theta_1$  to  $\theta_1$  lagging behind  $\theta_2$ ); and (c) variation of the selection signal (from 0 to 1) and variation of the angular position (from  $\theta_1$  lagging behind  $\theta_2$  to  $\theta_2$  lagging behind  $\theta_1$ ).

#### 4.3. Dynamic Performance Experiment

To verify the effectiveness of the proposed SMC speed control scheme, the dynamic performance of the motor system experiments were carried out through the experiment set-up. Experiments were conducted to evaluate the effectiveness of the proposed SMC speed control scheme under various operating conditions, including sudden load and sudden unload conditions. Therefore, the results of the traditional PI speed control were compared with the results of the proposed SMC speed control under the same conditions. Both of the current controllers adopted the PI control scheme; however, the speed controller adopted the SMC or the PI control scheme. When the PI control scheme was

adopted, the parameters of the speed controller were  $k_{ps} = 2.3$  and  $k_{is} = 12$ . The parameters of the two PI current controllers were the same:  $k_{pc} = 10$  and  $k_{ic} = 3.5$ .

Figure 9a,b show that the sudden load or unload experiments were done when the proposed motor ran at the nominal speed of 600r/min. The load torques of both of the rotors were changed simultaneously (from 10 Nm to 5 Nm and back again to 10 Nm). It can be concluded that the fluctuations of the speed controlled by the SMC speed control method were much smaller than that of the motor system controlled by the conventional PI speed control strategy. Figure 9c,d show that the command speed was changed from 600 r/min to 300 r/min and then back to 600 r/min. It was obvious that the torques of both the rotors fluctuated during the speed transitions. But the fluctuations of the torque under the SMC speed control condition were much smaller than that of the system under the conventional PI speed control condition. From Figure 9, it can be concluded that the SMC speed controller can improve the dynamic performance and enhance the disturbance suppression ability of the motor system compared with the PI speed controller. Simultaneously, the robustness and the stability of the motor system can be ensured through adopting the SMC control strategy.

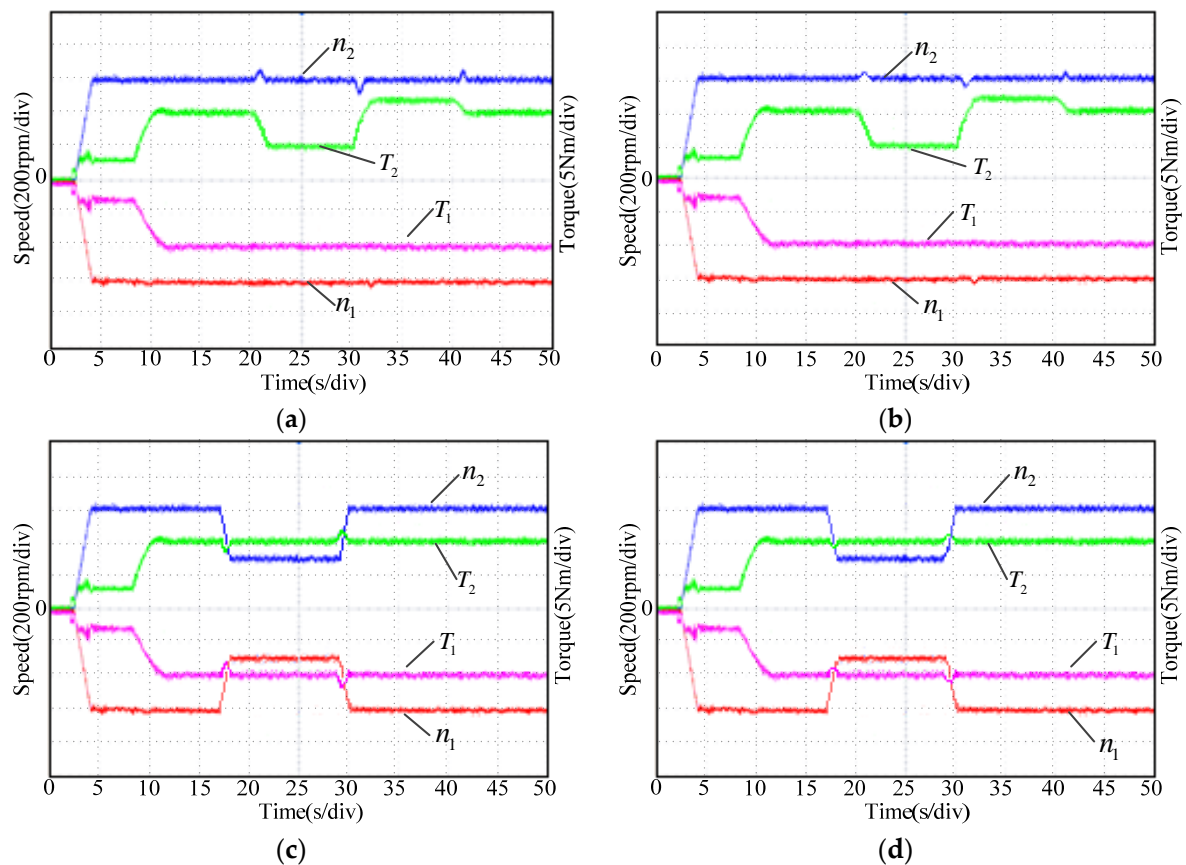


**Figure 9.** The dynamic performance of the system under PI or SMC speed control. (a) Torque and speed response based on PI speed control (only load 2 changes); (b) torque and speed response based on SMC speed control (only load 2 changes); (c) torque and speed response based on PI speed control (the speed command changes); and (d) torque and speed response based on SMC speed control (the speed command changes).

## 5. Conclusions

In this paper, one nonlinear SMC speed control technique for a permanent magnet synchronous motor with dual-rotating rotors has been proposed in order to design a robust speed controller. The proposed scheme was implemented by using DSP TMS320F28335. The major contributions of this work include: (i) The mathematic model of the PMSM with dual-rotating rotors was developed;

(ii) in the case of an unbalanced load, how to select the main motor to ensure the stability of the system was analyzed; (iii) the SMC speed controller was presented; and (iv) the successful application and comparative results demonstrated that the proposed control method was effective and, accordingly, the methodology proposed in this work can be applied to the propeller drive system with dual-rotating rotors.

**Author Contributions:** Y.Z. and S.H. conceived and designed the proposed topology and control methodology. Yichang Zhong performed experimental analysis, and modeling and simulation. D.L. and Y.Z. significantly contributed to the analysis of the experiment and the writing—original draft preparation, writing—review & editing and the writing of the paper.

**Funding:** This research was funded by National Natural Science Foundation of China under Project 51577052 and National Key Research and Development Program of China under Project 2016YFF0203400.

**Conflicts of Interest:** The authors declare no conflicts of interest.

## References

1. Nakai, H.; Ohtani, H.; Satoh, E.; Inaguma, Y. Development and testing of the torque control for the permanent-magnet synchronous motor. *IEEE Trans. Ind. Electron.* **2005**, *52*, 800–806. [[CrossRef](#)]
2. Chang, S.H.; Chen, P.Y.; Ting, Y.H.; Hung, S.W. Robust current control-based sliding mode control with simple uncertainties estimation in permanent magnet synchronous motor drive systems. *IET Electr. Power Appl.* **2010**, *4*, 441–450. [[CrossRef](#)]
3. Boldea, T.; Tutelea, L.N.; Deaconu, S.T.; Marignetti, F. Dual rotor single-stator axial air gap PMSM motor/generator drive for REVs: A review of comprehensive modeling and performance characterization. In Proceedings of the 2012 Electrical Systems for Aircraft, Railway and Ship Propulsion (ESARS), Bologna, Italy, 16–18 October 2012.
4. Qu, R.H.; Lipo, T.A. Dual-rotor, radial-flux, toroidally wound permanent-magnet machines. *IEEE Trans. Ind. Appl.* **2003**, *39*, 1665–1673.
5. Xu, L.; Zhang, Y.; Wen, X. Multioperational modes and control strategies of dual-mechanical-port machine for hybrid electrical vehicles. *IEEE Trans. Ind. Appl.* **2009**, *45*, 747–755. [[CrossRef](#)]
6. Pisek, P.; Stumberger, B.; Marcic, T.; Virtic, P. Design analysis and experimental validation of a double rotor synchronous PM machine used for HEV. *IEEE Trans. Magn.* **2013**, *49*, 152–155. [[CrossRef](#)]
7. Zhang, Z.; Chau, K.T.; Wang, Z. Chaotic speed synchronization control of multiple induction motors using stator flux regulation. *IEEE Trans. Magn.* **2012**, *48*, 4487–4490. [[CrossRef](#)]
8. Wu, B.; Dewan, S.B.; Sen, P.C. A modified current source inverter (MCSI) for a multiple induction motor drive system. *IEEE Trans. Power Electr.* **1988**, *3*, 10–16. [[CrossRef](#)]
9. Zhao, D.Z.; Li, C.W.; Ren, J. Speed synchronisation of multiple induction motors with adjacent cross-coupling control. *IET Control Theory Appl.* **2010**, *4*, 119–128. [[CrossRef](#)]
10. Yeager, K.E. Bus transfer of multiple induction motor loads in a 400 megawatt fossil power plant. *IEEE Trans. Energy Convers.* **1988**, *3*, 451–457. [[CrossRef](#)]
11. Hu, J.J.; Zheng, L.L.; Jia, M.X.; Zhang, Y.; Pang, T. Optimization and model validation of operation control strategies for a novel dual-motor coupling-propulsion pure electric vehicle. *Energies* **2018**, *11*, 754. [[CrossRef](#)]
12. Qin, C.Y.; Zhang, C.N.; Lu, H.Y. H-shaped multiple linear motor drive platform control system design based on an inverse system method. *Energies* **2017**, *10*, 1990. [[CrossRef](#)]
13. Bidart, D.; David, M.P.; Maussion, P.; Fadel, M. Mono inverter multi-parallel permanent magnet synchronous motor: Structure and control strategy. *IET Electr. Power Appl.* **2011**, *5*, 288–294. [[CrossRef](#)]
14. Wei, C.; Liang, J.J.; Shi, T.N. Speed synchronous control of multiple permanent magnet synchronous motors based on an improved cross-coupling structure. *Energies* **2018**, *11*, 282. [[CrossRef](#)]
15. Chiasson, J.; Seto, D.; Sun, F.; Stankovic, A.; Bortoff, S. Independent control of two PM motors using a single inverter application to elevator doors. In Proceedings of the 2002 American Control Conference (ACC), Anchorage, AK, USA, 8–10 May 2002.
16. Cheng, S.Y.; Luo, D.R.; Huang, S.D.; Chen, Z.; Huang, K.Y. Control strategy for permanent magnet synchronous motor with contra-rotating rotors under unbalanced loads condition. *IET Electr. Power Appl.* **2015**, *9*, 71–79. [[CrossRef](#)]

17. Zhong, Y.C.; Huang, S.D.; Luo, D.R.; He, R.Z. Speed synchronism of permanent magnet synchronous motor with dual contra-rotating rotors under load variation. *IET Power Electron.* **2017**, *10*, 1479–1486. [[CrossRef](#)]
18. Wu, S.; Wang, Y.; Cheng, S. Optimal reset control design for current control and uncertainties estimation in permanent magnet synchronous. *IET Electr. Power Appl.* **2012**, *6*, 122–132. [[CrossRef](#)]
19. Hsien, T.L.; Sun, Y.Y.; Tsai, M.C.  $H_\infty$  control for a sensorless permanent-magnet synchronous drive. *IEE Proc. Electr. Power Appl.* **1997**, *144*, 173–181. [[CrossRef](#)]
20. Feng, G.; Liu, Y.F.; Huang, L.P. A new robust algorithm to improve the dynamic performance on the speed control of motor drive. *IEEE Trans. Power Electron.* **2004**, *19*, 1614–1627. [[CrossRef](#)]
21. Zhang, X.G.; Sun, L.Z.; Zhao, K.; Sun, L. Nonlinear speed control for PMSM system using sliding-mode control and disturbance compensation techniques. *IEEE Trans. Power Electron.* **2013**, *28*, 1358–1365. [[CrossRef](#)]
22. Wang, A.M.; Jia, X.W.; Dong, S.H. A new exponential reaching law of sliding mode control to improve performance of permanent magnet synchronous motor. *IEEE Trans. Magn.* **2013**, *49*, 2409–2412. [[CrossRef](#)]
23. Li, S.H.; Zhou, M.M.; Yu, X.H. Design and implementation of terminal sliding mode control method for PMSM speed regulation system. *IEEE Trans. Ind. Inf.* **2013**, *9*, 1879–1891. [[CrossRef](#)]
24. Chen, C.S. TSK-type self-organizing recurrent-neural-fuzzy control of linear microstepping motor drives. *IEEE Trans. Power Electron.* **2010**, *25*, 2253–2265. [[CrossRef](#)]
25. Singh, M.; Chandra, A. Application of adaptive network-based fuzzy inference system for sensorless control of PMSG-based wind turbine with nonlinear-load-compensation capabilities. *IEEE Trans. Power Electron.* **2011**, *26*, 165–175. [[CrossRef](#)]
26. Liu, J.; Li, H.W.; Deng, Y.T. Torque ripple minimization of PMSM based on robust ILC via adaptive sliding mode control. *IEEE Trans. Power Electron.* **2018**, *33*, 3655–3671. [[CrossRef](#)]
27. Flieller, D.; Nguyen, N.K.; Wira, P. A self-learning solution for torque ripple reduction for nonsinusoidal permanent magnet motor drives based on artificial neural networks. *IEEE Trans. Ind. Electron.* **2014**, *61*, 655–666. [[CrossRef](#)]
28. Sun, X.D.; Chen, L.; Jiang, H.B.; Yang, Z.B.; Chen, J.F.; Zhang, W.Y. High-performance control for a bearingless permanent-magnet synchronous motor using neural network inverse scheme plus internal model controllers. *IEEE Trans. Ind. Electron.* **2016**, *63*, 3479–3488. [[CrossRef](#)]
29. Sun, X.D.; Shi, Z.; Chen, L.; Yang, Z.B. Internal model control for a bearingless permanent magnet synchronous motor based on inverse system method. *IEEE Trans. Energy Convers.* **2016**, *31*, 1539–1548. [[CrossRef](#)]
30. Sun, X.D.; Chen, L.; Yang, Z.B.; Zhu, H.Q. Speed-Sensorless Vector Control of a Bearingless Induction Motor with Artificial Neural Network Inverse Speed Observer. *IEEE Trans. Mechatron.* **2013**, *18*, 1357–1366. [[CrossRef](#)]
31. Chen, B.S. *Power Electronics and Electric Drive Automation—Compilation of Important Papers of Prof. Chen Boshi*; China Machine Press: Beijing, China, 2008; pp. 40–61. ISBN 978-7-111-23986-4.

